Review

Journal of Molecular Recognition

Received: 17 June 2013, Revised: 14 August 2013, Accepted: 15 August 2013, Published online in Wiley Online Library

(wileyonlinelibrary.com) DOI: 10.1002/jmr.2311

DNA substrate preparation for atomic force microscopy studies of protein–DNA interactions

Claudia N. Buechner and Ingrid Tessmer*

Protein–DNA interactions provide fundamental control mechanisms over biologically essential processes such as DNA replication, transcription, and repair. However, many details of these mechanisms still remain unclear. Atomic force microscopy (AFM) analyses provide unique and important structural and functional information on such protein–DNA interactions at the level of the individual molecules. The high sensitivity of the method with topographical visualization of all sample components also demands for extremely clean and pure materials. Here, we provide an overview of molecular biology-based approaches to produce DNA substrates for AFM imaging as well as other types of experiments, such as optical or magnetic tweezers, that profit from controllable substrate properties in long DNA fragments. We present detailed strategies to produce different types of motifs in DNA that are frequently employed targets of protein interactions. Importantly, the presented preparation techniques imply exact knowledge of the location of the introduced specific target sites within the DNA fragments, allowing for a distinction between specific and non-specific protein–DNA interactions in the AFM images and for separate conformational analyses of the different types of protein–DNA complexes. Copyright © 2013 John Wiley & Sons, Ltd.
Additional supporting information may be found in the online version of this article at the publisher's web site.

Keywords: DNA substrate preparation; DNA modification; protein–DNA interactions; DNA repair; atomic force microscopy (AFM); single molecule imaging

INTRODUCTION

DNA modifications play essential roles *in vivo*. The stability of DNA is constantly chemically and physically threatened, often resulting in broken, otherwise structurally altered, or chemically modified DNA (Hoeijmakers, 2001). Chemical modifications are also introduced specifically into DNA, for instance cytosine methylation by the methyltransferase enzymes, as a signal for protein interactions involved in transcription and replication regulation (Okano *et al*., 1999; Johnson *et al*., 2012). Specific structural features in the DNA serve as target sites for protein binding. For instance, DNA repair proteins responsible for initial damage detection in DNA mismatch repair and nucleotide excision repair pathways are believed to recognize DNA helix distortions and changes in DNA flexibility (Sugasawa *et al*., 2001; Yang *et al*., 2005; Tessmer *et al*., 2008; Yang, 2008).

Different types of DNA structures can be mimicked by artificially prepared DNA substrates. For instance, the introduction of short stretches of unpaired DNA bases within duplex DNA represents a convincing model of the biologically essential DNA intermediates that form during transcription and replication, the so-called transcription or replication bubble, as well as during DNA repair (Zou *et al*., 1997; Orphanides and Reinberg, 2002; Sugasawa *et al*., 2009). Many DNA-processing enzymes specifically target the junctions of single stranded DNA (ssDNA) and double stranded DNA (dsDNA) (Declais and Lilley, 2008; Roth *et al*., 2012). SsDNA structures are also preferentially bound by proteins such as the functional class of ssDNA binding proteins (e.g., ssDNA-binding protein (SSB) and replication protein A) that protect the fragile ssDNA intermediates of DNA processing *in vivo* (Kelly *et al*., 1998; Liu *et al*., 2005a; Sanchez *et al*., 2008). For the study of DNA repair processes, specific types of lesions can be artificially introduced in DNA to provide model structures allowing the *in vitro* analysis of their processing by the relevant proteins (Zou *et al*., 1997; Verhoeven *et al*., 2001; Chen *et al*., 2002; Janicijevic *et al*., 2003b; Wang *et al*., 2003; Hou *et al*., 2007; Tessmer *et al*., 2008; Sugasawa *et al*., 2009). Furthermore, DNA fragment ends directly serve as target sites of proteins involved in DNA double strand break (DSB) repair (Moreno-Herrero *et al*., 2005; Wu *et al*., 2006).

Imaging by atomic force microscopy (AFM) is a highly attractive approach for the study of structural effects of DNA modifications *per se* (Shlyakhtenko *et al*., 2000; Tiner *et al*., 2001; Brezeanu *et al*., 2007; Gudowska-Nowak *et al*., 2009; Zhang *et al*., 2009; Wang *et al*., 2010) as well as their recognition and processing by specialized sets of protein machineries (Chen *et al*., 2002; Janicijevic *et al*., 2003b, 2003a; Wang *et al*., 2003; Yang *et al*., 2003; Yang *et al*., 2005; Tessmer *et al*., 2008; Shlyakhtenko *et al*., 2012a, 2012b). Similarly, electron microscopy (EM) is a well-established tool for the investigation of DNA topologies (Cunningham *et al*., 1980; Wasserman and Cozzarelli, 1986) and protein–DNA complexes (Shi *et al*., 1992; Nossal *et al*., 2007) in recombination and replication processes. While EM images afford slightly higher resolution than AFM, which is limited by convolution of sample topography with the AFM imaging probe (Winzer *et al*., 2012), advantages of AFM over EM as well as other

* *Correspondence to: Ingrid Tessmer, Rudolf Virchow Center for Experimental Biomedicine, Josef Schneider Str. 2, 97080 Würzburg, Germany.*
E-mail: ingrid.tessmer@virchow.uni-wuerzburg.de

C. N. Buechner, I. Tessmer
Rudolf Virchow Center for Experimental Biomedicine, University of Wuerzburg, Josef Schneider Str. 2, 97080 Wuerzburg, Germany

high resolution techniques include the rapid and easy experimental sample preparation (section Sample Preparation for Atomic Force Microscopy Imaging of Protein–DNA Samples). Furthermore, AFM imaging does not require staining of samples avoiding the introduction of background and artifacts. Importantly, AFM allows for the direct imaging of fully hydrated molecules in near-physiological, liquid environment (sections Sample Preparation for Atomic Force Microscopy Imaging of Protein–DNA Samples and Atomic Force Microscopy Imaging Experiments on Protein–DNA Systems), strengthening the possibility of the native structure of biological particles to be conserved in the images.

Atomic force microscopy experiments provide unique insight into structural and functional parameters of protein–DNA interactions at the single molecule level (Bustamante and Rivetti, 1996; Janicijevic *et al*., 2003a; Pastre *et al*., 2010; Billingsley *et al*., 2012a). The high sensitivity of the method with nanometer resolution and topographical visualization of all sample components also demands for extremely clean and pure materials. While protein purification methods by liquid chromatography are well established, the expertise for suitable DNA substrate preparation is generally not as prevalent. A major advantage of AFM investigations (as well as imaging by EM) over most other biophysical and biochemical approaches is the possibility to use long DNA substrates of hundreds to thousands of base pairs (bp) length. Long DNA substrates provide targets for protein binding that more closely match physiological conditions than the short DNA oligomers typically employed in most protein–DNA interaction assays. For instance, they can stabilize tertiary structures such as DNA loops and minimize interfering effects of DNA ends on protein binding.

For unambiguous analyses, protein–DNA studies require a distinct knowledge of and control over DNA substrate properties such as the exact position and character of the target site for the protein. Different schemes have been applied for the preparation of long DNA substrates that contain a particular target site for a protein under investigation and are suitable for AFM experiments (Verhoeven *et al*., 2001; Chen *et al*., 2002; Janicijevic *et al*., 2003b; Wang *et al*., 2003; Hou *et al*., 2007; Sugasawa *et al*., 2009; Myong and Ha, 2010; Luzzietti *et al*., 2011; Luzzietti *et al*., 2012). These preparations involve two essential parts: (i) the reliable and homogeneous introduction of the target site or structure of choice into the DNA; and (ii) the careful purification of the final, clean DNA product. We will detail these two important aspects of DNA substrate preparation for AFM in the next two sections, providing simple guidelines, controls, and examples. Finally, we will demonstrate the principle and power of AFM studies of protein interactions using long DNA substrates containing specific sites in example applications.

INTRODUCTION OF SPECIFIC DNA SITES INTO LONG DNA SUBSTRATES

DNA fragments of a few hundred to several thousand base pairs length can be produced via polymerase chain reaction (PCR) or from a DNA plasmid, transformed into and amplified in *E. coli* cells (as, for instance, detailed in (Green and Sambrook, 2012)). In contrast to PCR, common laboratory strains of *E. coli* introduce postreplicative base modifications in DNA (Marinus, 1987; Barras and Marinus, 1989). However, DNA methylation patterns in eukaryotes differ from those produced in prokaryotes, and the different modification context may interfere with some protein–DNA interactions (Barras and Marinus, 1989; Jeltsch, 2002). Where required, (DAM (DNA adenine methylation)/DCM (DNA cytosine methylation) negative) *E. coli* strains that do not introduce DNA methylation are therefore available (Palmer and Marinus, 1994). The amplified plasmid DNA can be extracted from the cells and purified using various strategies, such as organic extraction via phenol-chloroform followed by ethanol precipitation, cesium chloride gradient centrifugation followed by dialysis, or silica-based column purification via commercially available kits (described, for example, in (Green and Sambrook, 2012)). Different types of specific target sites for protein interactions can then be incorporated into these long DNA substrates, as described in the following sub-sections.

DNA base sequences

Many biologically relevant proteins (restriction endonucleases, transcription factors, etc.) possess high specificity for binding to particular DNA base recognition sequences. In terms of DNA substrate preparation, this type of specific site is the trivial case and the exact location of the sequence within the entire DNA context is known from the plasmid map. In some cases, the introduction of a particular sequence via site-directed mutagenesis may be required (Aiyar *et al*., 1996). More intricately, Seeman and colleagues used restriction digest to replace entire stretches of a circular plasmid with sequences identical to those found elsewhere in the DNA, to investigate the effects of homologous sequences on DNA superstructure (see also next sub-section) (Wang *et al*., 2010).

DNA structures

Often, protein interactions are targeted to specific structural features in the DNA, such as different types of DNA superstructure, fragment ends, forks, flaps, or bubbles, which involve ss/dsDNA junctions, or ssDNA regions. Alternative superstructures to B-form DNA, such as partial triplex DNA (H-DNA) or different supercoiled DNA isoforms including left-handed (Z-)DNA induced by negative supercoiling, have been proposed to be involved in DNA transcription, replication, and recombination (Rich *et al*., 1984; Mirkin and Frankkamenetskii, 1994).

(i) DNA superstructures

Various proteins preferentially recognize and interact with supercoiled DNA as demonstrated by AFM (Lushnikov *et al*., 2004; Roth *et al*., 2012) as well as biochemical analyses (Butler, 1986; Slocum *et al*., 2007). To study specificities for particular isoforms of supercoiled DNA, distinct supercoiling states can be produced from supercoiled plasmid DNA by incubation with topoisomerase and be isolated using extraction from agarose gel electrophoresis. Different research groups have used AFM to study DNA structural transitions in circular plasmid DNA that are induced by the presence of alternating pyrimidine–purine sequences or long inverted repeats of oligo-pyrimidine/oligo-purine sequences (Shlyakhtenko *et al*., 2000; Tiner *et al*., 2001; Wang *et al*., 2010) and are believed to be targets of specific protein interactions (Rich *et al*., 1984; Mirkin and Frankkamenetskii, 1994). For these studies, higher order, four-stranded DNA superstructures with left-handed chirality were produced by inserting dsDNA stretches of repeat

sequences into pUC19 plasmid DNA (Wang *et al*., 2010). Homopurine and homopyrimidine sequence stretches that form hydrogen ion stabilized intramolecular triplex DNA structures (H-DNA), which likely possess important biological functions *in vivo* (Mirkin and Frankkamenetskii, 1994), have been cloned into the EcoRI site of pUC19 (Blaszak *et al*., 1999). The resulting transitions to H-form DNA could be visualized by AFM (Tiner *et al*., 2001). In addition, three-way DNA junctions mimicking recombination and replication intermediates can, for instance, be artificially introduced into dsDNA by denaturing DNA fragments, which differ only in that one of them contains a short additional insert sequence, followed by mixed annealing to form heteroduplex hybrids (Shlyakhtenko *et al*., 2000).

(ii) DNA double strand breaks

DNA DSBs are conveniently mimicked by the ends of linear DNA fragments, which can hence be directly used as substrates in studies on protein systems involved in DSB repair (Ristic *et al*., 2003; Moreno-Herrero *et al*., 2005; Wu *et al*., 2006). The choice of restriction enzyme used for plasmid linearization allows for easy control of the blunt or ssDNA overhang nature of the fragment ends.

(iii) Single stranded–double stranded junctions

Single stranded/double stranded DNA junctions can be represented experimentally by DNA fragments containing short 3′ or 5′ single-stranded overhangs, where proteins can often clearly and specifically distinguish between these two different substrates (Roth *et al*., 2012). If only short ssDNA overhangs of typically ≤5 bases are required, many polymerases automatically produce 3′ ssDNA-overhangs in PCR products, for instance the Taq or 7 ac7 DNA polymerases (Hu, 1993). However, the degree of efficiency with which these overhangs are added varies, and even enzymes with a high, so-called, extendase activity do not achieve homogeneous populations of ssDNA overhangs (Hu, 1993). Alternatively, PCR fragments as well as plasmid DNA can be digested with an appropriate restriction enzyme to produce short (few nucleotides) 3′ or 5′ overhangs (Tessmer *et al*., 2005). A simple approach for the generation of DNA fragments with longer 3′ or 5′ ssDNA overhangs is based on the incision of one of the strands of a PCR product with an appropriate nickase, a short distance away from the DNA fragment ends followed by heat denaturation (Roth *et al*., 2012), as illustrated schematically in Figure 1 and as detailed in the Supporting Information. The choice of nick position depends on the desired length of ssDNA overhangs. Alternatively, long complementary ssDNA strands of differing length can be annealed resulting in linear dsDNA substrates containing an ssDNA overhang. For the production of long ssDNA, different approaches can be employed (evaluated in (Civit *et al*., 2012)), for instance, treatment with lambda exonuclease or coupled alkaline/temperature induced denaturation of biotinylated DNA immobilized on and subsequently isolated via streptavidin-coated magnetic beads. Furthermore, Lyubchenko and co-workers have developed an elegant method to produce DNA fragments with long (≤69 nucleotides (nt)) ssDNA overhangs (tail-DNA) by annealing restriction enzyme digested PCR products (230–440 bp) and the ssDNA oligonucleotide via an ssDNA adaptor structure (Shlyakhtenko *et al*., 2011; Shlyakhtenko *et al*., 2012a, 2012b).

Similar procedures can also be employed to produce DNA containing an internal single-stranded region (gap-DNA).

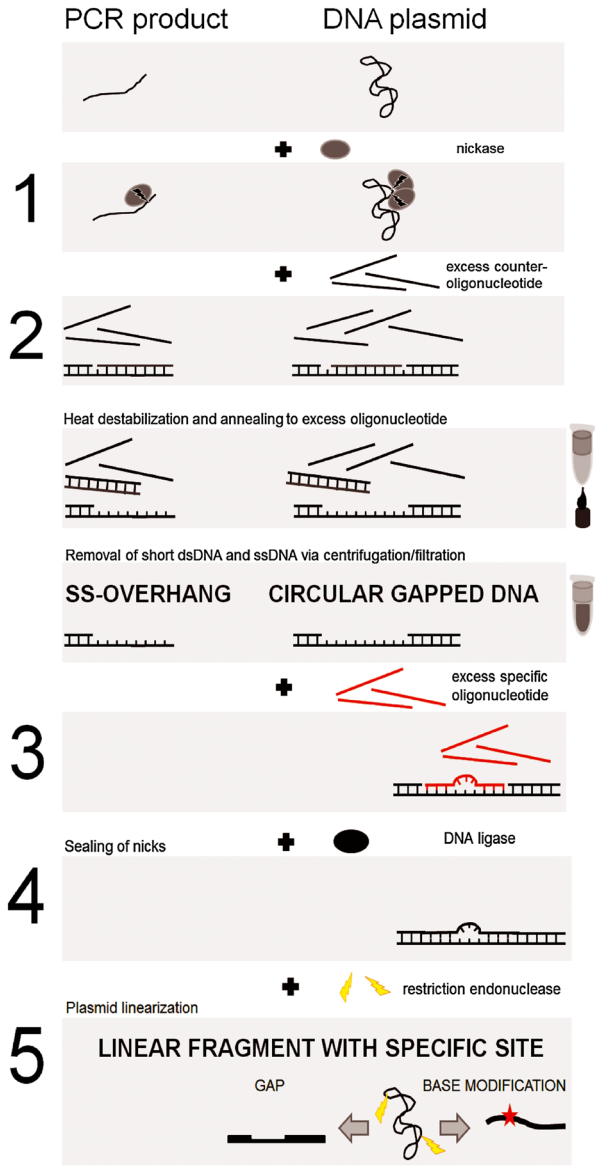

Figure 1. Schematic of DNA substrate preparation: preparation of ssDNA overhangs (section DNA structures), internal ssDNA gaps (section DNA structures), and internal DNA modifications (method 4, section Chemical DNA modifications) using a nicking endonuclease. (1) Polymerase chain reaction fragments or plasmid DNA are incised on one of the DNA strands by incubation with a nicking restriction enzyme (grey oval). (2) An excess of DNA counter-oligonucleotide to the short ssDNA stretch separated by the nickase site(s) is applied (black lines). The sample is heated to induce melting of the ssDNA stretch from the original DNA molecule. Upon cooling, the ssDNA stretch preferentially anneals with the excess oligonucleotide complement. The annealed dsDNA oligos as well as the excess ssDNA oligos are removed in a filtration step, resulting in linear fragments with ssDNA overhangs or gapped circular DNA. (3) If the insertion of a modified oligonucleotide (containing specific target structures) into the gapped region is desired, the oligonucleotide is applied in excess (red lines) and anneals with the gapped region in the DNA, to which it is complementary. (4) The remaining nicks between the newly inserted DNA oligo and the original DNA are sealed by incubation with DNA ligase (black oval). (5) In the final step, DNA fragments of the desired length containing the specific site (either an ssDNA gap or a DNA modification = red star) are produced from the long circular DNA substrate by digestion with the appropriate restriction enzymes (yellow flesh). The linear polymerase chain reaction fragments are typically already of a length suitable for atomic force microscopy experiments.

Lyubchenko and colleagues again used ssDNA adaptors to ligate 5′ and 3′ single stranded tail-DNAs together, producing long (several hundred base pairs) dsDNA fragments containing internal 69 nt long ssDNA gaps (Shlyakhtenko *et al*., 2012a, 2012b). Alternatively, Figure 1 describes the introduction of an internal ssDNA gap region within long plasmid DNA based on the application of a nicking endonuclease. The ssDNA stretches between the resulting DNA nicks can be removed, for instance, by thermal denaturation. Several approaches based on different plasmids and slightly varying procedures have been reported in the literature (Hou *et al*., 2007; Pyle, 2008; Geng *et al*., 2011; Luzzietti *et al*., 2011; Luzzietti *et al*., 2012), and an explicit example protocol is detailed in the Supporting Information. This nickase-based production of internal ssDNA gaps within long (linear or circular) dsDNA is a relatively simple, fast, and efficient approach. In addition, it provides an innate restriction enzyme digest control option to confirm completeness of DNA gapping (see section Controls of DNA Substrate Preparations).

Chemical DNA modifications

Specific types of lesions, other chemical base modifications, or base–base mismatches can be introduced in DNA at a defined position to provide target sites for protein interactions. Different schemes have been applied for the preparation of such DNA substrates (Sugasawa *et al*., 2001; Verhoeven *et al*., 2001; Chen *et al*., 2002; Janicijevic *et al*., 2003a; Hou *et al*., 2007; Tessmer *et al*., 2008; Sugasawa *et al*., 2009; Wagner *et al*., 2009; Geng *et al*., 2011; Luzzietti *et al*., 2011), all of which are based on ligating a specific target site containing short stretch of DNA into a longer DNA context. We will detail the different established approaches in the next paragraphs.

Basically, the specific DNA modification can either be integrated into longer DNA sequences as part of a short dsDNA fragment or as an ssDNA oligonucleotide. In the first scenario (method 1) (Wang *et al*., 2003; Tessmer *et al*., 2008), three separate dsDNA fragments were ligated together using overlapping 3-nucleotide ssDNA overhangs to produce a long DNA substrate. The two outer dsDNA fragments were produced via PCR. Importantly, the central of the three segments was a polyacrylamide gel purified short (~80 bp) dsDNA fragment that contained the target site(s) of choice at a defined position. This approach has been used for the production of long DNA substrates containing a DNA base mismatch, but can of course in principle be employed for the introduction of any type of specific target site. This strategy resembles that described previously for the production of gapped DNA substrates (which could similarly be modified and applied here) developed by Lyubchenko and colleagues (Shlyakhtenko *et al*., 2012a, 2012b) with the short ssDNA overhangs directly acting as the bridging structures.

In the second scenario, specific target site containing ssDNA oligonucleotides are annealed to complementary DNA sequences within longer DNA strands. Different variations on this theme have been reported (methods 2–4). Firstly, annealing of the modification-carrying oligonucleotide can be in a linear or a circular DNA context. The approach based on linear PCR products (method 2) has first been described by Verhoeven and colleagues and has been applied to the preparation of DNA substrates containing menthol and cholesterol modifications (Verhoeven *et al*., 2001; Janicijevic *et al*., 2003a; Wagner *et al*., 2009). This method uses streptavidin-coated magnetic beads to isolate melted biotinylated ssDNA fragments of several hundred to ~1000 bp as well as shorter complementary ssDNA fragments from PCR products. The shorter ssDNA strand was annealed to the long ssDNA fragment immobilized by the magnetic beads, together with the commercially obtained oligonucleotide containing the specific modification. The modified oligonucleotide then served as primer in the following step, in which polymerase, deoxyribonucleoside triphosphates, and ligase were added to the reaction to complete the complementary strand and seal the nicks. Finally, the complete dsDNA strand containing the modification at a defined position could be released from the magnetic beads by digestion with a suitable restriction enzyme.

The third approach employs circular plasmid DNA as a template for the integration of specific site containing DNA. Two different strategies are based on either ssDNA phagemids (method 3) or dsDNA plasmids (method 4). In method 3, ssDNA phagemids such as pBS + or pBluescript II KS(+) have been amplified via helper phage procedure and used as template for annealing of a short modification-containing oligonucleotide (Sugasawa *et al*., 2001; Chen *et al*., 2002; Sugasawa *et al*., 2009). Similar as in method 2, the oligonucleotide then served as primer. Polymerase and ligase were added to synthesize fully double-stranded, intact (nick-free) circular DNA. Finally, restriction digests produce linear DNA fragments containing the specific target site at a well-known position. This approach has been exploited in the study of DNA repair proteins on 8-oxoguanine adducted DNA (Chen *et al*., 2002) or DNA containing a site-specific UV photo or 2-acetylaminofluorene lesion (Sugasawa *et al*., 2001; Sugasawa *et al*., 2009). In contrast to the latter variant, method 4 uses pUC19-based dsDNA plasmids (Hou *et al*., 2007; Geng *et al*., 2011; Luzzietti *et al*., 2011). The plasmids were modified to contain various close restriction sites for a nicking endonuclease, following standard cloning procedures (Wang and Hays, 2000; Wang and Hays, 2001; Luzzietti *et al*., 2011). The nickase cuts only one of the DNA strands, and the short ssDNA stretch between the nicks can then be thermally destabilized and removed from the plasmid in the presence of an excess of counter-oligonucleotide. Into the resulting gap, an oligonucleotide containing the specific modification can then be ligated. As aforementioned, final DNA substrates containing the target site(s) of choice at a well-defined position are achieved by restriction enzyme digest. This approach has been applied to the introduction of DNA base mismatches and methylated bases (Geng *et al*., 2011), biotinylation sites for the attachment of nanoparticles or even entire internal tertiary DNA structures (Luzzietti *et al*., 2011), uracil (Hou *et al*., 2007), and fluorescein adducts (Figures 2 and 3(A)) (own unpublished data). In lieu of all of these DNA substrate preparation approaches (methods 1–4), in the Supporting Information, we provide a detailed protocol for the last method (method 4; DNA substrate preparation based on modified dsDNA plasmid), which is also schematically outlined in Figure 1.

All of these methods are well suited to produce DNA substrates containing specific modifications at well-defined sites with high homogeneity. Substrate yields may vary between the different approaches; they are, however, mainly dominated by the following necessary purification procedures (section Controls of DNA Substrate Preparations) rather than the different methods for introducing DNA modifications. Both PCR and amplification of phagemid/plasmid DNA can produce large amounts of initial DNA template. Also, the yield of final modified substrate from the initial DNA template is typically high and is further supported

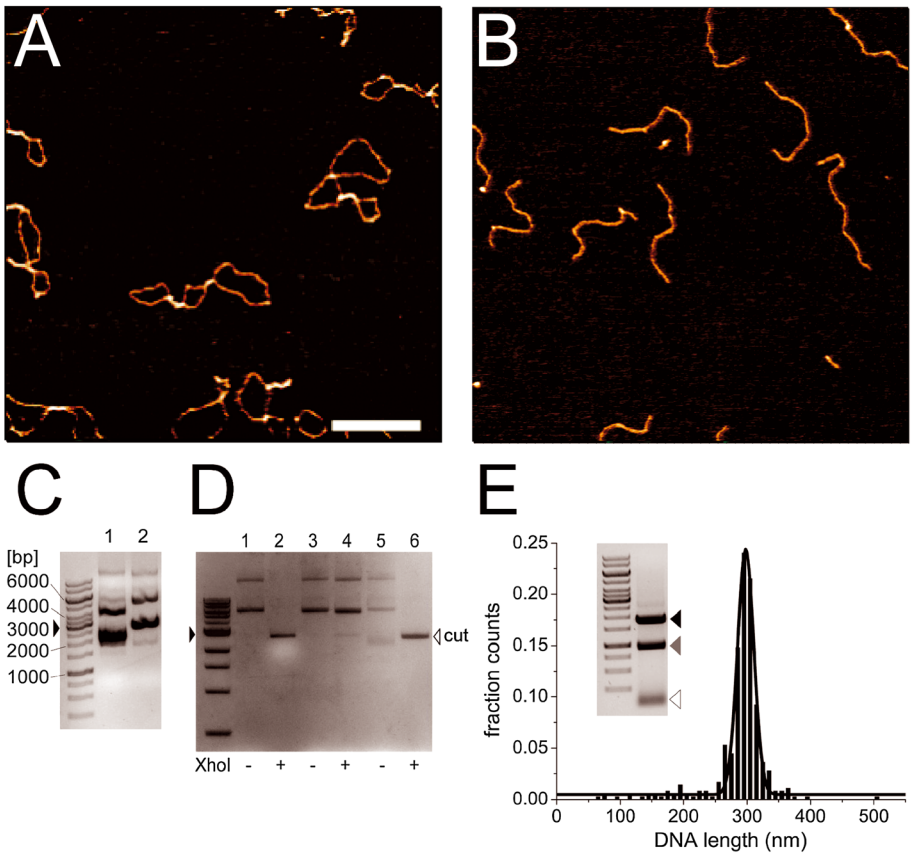

Figure 2. Assaying substrate preparation. DNA substrates need to be extremely clean and homogeneous for atomic force microscopy (AFM) imaging experiments, in which the identification and optimum resolution of small DNA-interacting particles are essential. (A) Circular plasmid DNA (2729 bp) and (B) linear DNA substrate (916 bp) containing a fluorescein modification within the context of a DNA bubble, after gel purification. The scale bar in (A) corresponds to 200 nm and both images are 1 μm × 1 μm. (C,D) Agarose gel-based enzyme assays to monitor DNA incisions and successful removal and replacement of specific oligomeric single stranded DNA (ssDNA) stretches. Bands were visualized by Midori Green staining. (C) Single strand cuts (nicks) in circular plasmid DNA can be observed in these assays based on the induced relaxation of DNA supercoiling and the resulting change in electrophoretic mobility of the DNA (lane 1 = supercoiled plasmid DNA, lane 2 = nicked plasmid DNA). (D) Removal and insertion of the ssDNA stretch between the nicks are tested by digestion with the restriction enzyme XhoI. The restriction site of the test enzyme XhoI is within the ssDNA sequence, which is removed during the substrate preparation. DNA incision only occurs for duplex DNA. We can hence use the inability or ability for DNA incision as an indicator for successful removal of the ssDNA stretch between the single strand cuts and for complete insertion of the replacement oligonucleotide, respectively. Lane 1/2 = nicked circular DNA; lane 3/4 = gapped DNA; lane 5/6 = ligated modified DNA substrate; after incubation in the absence or presence of XhoI, as indicated. The bold arrowhead points at the same DNA marker position (3000 bp) as in (C); the white arrowhead indicates the running position of incised and hence linearized DNA. (E) Measurement of DNA lengths ($n = 358$) from AFM images reveals good homogeneity of the final DNA substrate. In the insert, black and grey arrows point at the gel electrophoresis bands of the two restriction digest products, the nonspecific homoduplex 1813 bp DNA fragment and the 916 bp fragment (containing the fluorescein/bubble) shown in (B), respectively. The white arrow indicates the applied excess insert oligo. A Gaussian fit to the length distribution of the 916 bp fragment shows a maximum at 298 nm (corresponding to 876 bp DNA) consistent with its theoretical length of 311 nm (with 0.34 nm/bp). The small deviation (–4%) from the theoretical length of the 916 bp fragment of 311 nm is likely due to small convolutions of the elastic DNA polymer strands that are not resolved in the AFM images. Typically, DNA fragment lengths measured from AFM images are ≤10% shorter than their calculated length. Homogeneity of the DNA sample is demonstrated by >75% of DNA fragment lengths being within two standard deviations from the center of the Gaussian fit.

by the application of a high (10-fold to 20-fold) excess of modification containing oligonucleotide for methods 2–4 (see for example Figure 2).

CONTROLS OF DNA SUBSTRATE PREPARATIONS

To be able to quantitatively interpret AFM data, it is essential that the DNA and protein samples are of high quality and do not contain any contaminating background species or major degree of heterogeneity within the substrate. For incubations with a DNA substrate containing a particular target for protein interactions, this requires that the specific site is present in the vast majority of applied DNA molecules (ideally >95%) at the designed position.

Different electrophoretic mobility of the DNA before and after modification can be exploited to test for successful substrate preparation, with numerous examples in the literature (Blaszak *et al*., 1999; Jiang *et al*., 2010; Wang *et al*., 2010; Fronczek *et al*., 2011; Luzzietti *et al*., 2011; Luzzietti *et al*., 2012). For instance, in method 4 for the introduction of specific DNA base modifications (described in sub-section Chemical DNA modifications, see also Supp. Information), an agarose-based electrophoretic mobility shift assay can serve to easily control the completion of each of the individual steps of the preparation. In this assay,

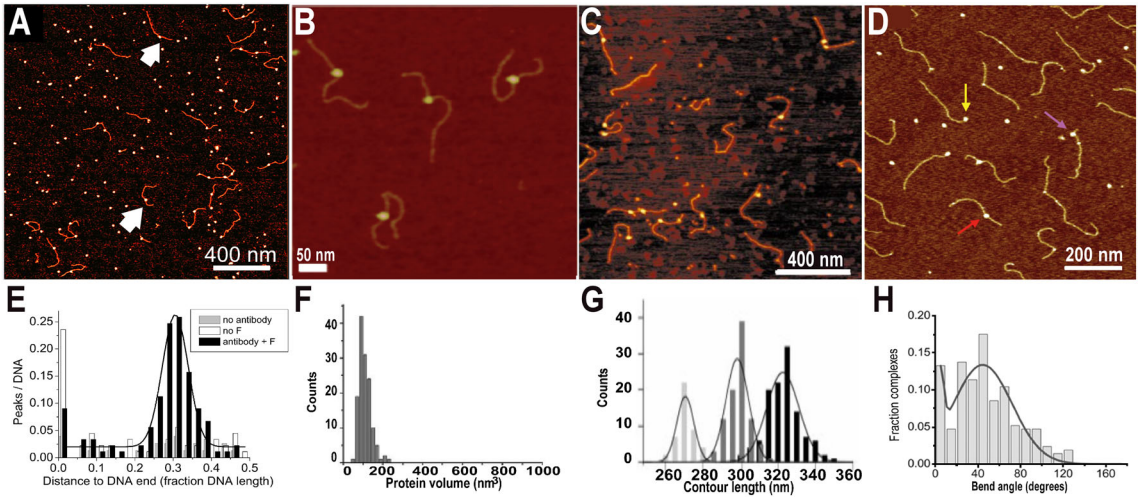

Figure 3. Atomic force microscopy (AFM) imaging of protein–DNA interactions. (A–D) AFM images of protein–DNA samples imaged in air. (E–H) Statistical analyses of protein–DNA complexes from A to D. (A) Fluorescein antibody with DNA containing a fluorescein modification in the context of a DNA bubble at ~31% of the DNA fragment length. Arrows indicate examples of antibody molecules bound to their target in the DNA. (B) Purified complexes of ssDNA binding protein bound to an ssDNA gap within long dsDNA fragments (Shlyakhtenko *et al.*, 2012b). (C) Purified heteromeric complexes of UvrA and UvrB bound to non-specific DNA fragments (Verhoeven *et al.*, 2001). (D) MutS complexes on DNA fragments containing a base mismatch at 27% of the DNA length (Tessmer *et al.*, 2008). Arrows indicate a protein complex bound specifically at a mismatch (red), non-specifically at a strand-internal, homoduplex position (purple), and at a DNA fragment end (yellow). (E) Position distribution of fluorescein antibody molecules on DNA containing a fluorescein target site (antibody + F, black bars, and fit line, $n = 112$ on 89 DNA fragments at ~31% DNA length). Recognition of its target by the antibody is obvious from the distinct Gaussian peak at this position in the distribution. In contrast, distributions obtained on the same fluorescein-DNA substrate in the absence of the antibody (grey bars, $n = 20$ on 76 DNA fragments), and for the antibody incubated with a DNA substrate that did not contain a fluorescein adduct (no F, white bars, $n = 61$ on 74 DNA fragments) show significantly less binding and are dominated by nonspecific complexes at random DNA positions and at DNA fragment ends. See Supplementary Figure S2 for AFM images of these negative controls. (F) Volume distribution for DNA bound ssDNA binding protein complexes shown in (B) (Shlyakhtenko *et al.*, 2012a, 2012b). (G) Distributions of contour lengths for DNA fragments shown in (C), with no protein bound (black bars), one UvrA-UvrB complex bound (dark grey bars), or two complexes bound (light grey bars) (Verhoeven *et al.*, 2001). (H) DNA bend angle distribution measured for MutS complexes ($n = 235$) bound specifically at the DNA mismatch position in (D) (Tessmer *et al.*, 2008). Two conformational states are apparent, one bent by ~50° and one straight (0° bending) complex.

the multiply nicked circular DNA (step 1 in Figure 1) can be distinguished from the non-nicked, negatively supercoiled plasmid DNA by its distinctly different mobility (compare lanes 1 and 2 in Figure 2(C)), similar as previously described (Luzzietti *et al.*, 2011). Complete removal and replacement of the ssDNA stretch between the DNA nicks (steps 2 and 3) can be assessed by digestion with a restriction enzyme, similar as previously described (Hou *et al.*, 2007). In the specific example shown in Figure 2, the restriction enzyme *XhoI* (NEB) requires intact dsDNA in the removed (48 nt) DNA sequence for incision, so that in the gapped intermediate, no incision can occur (compare lanes 3 and 4 and 5 and 6 in Figure 2(D)). Once successful introduction of the target site of choice has been confirmed, again by *XhoI* restriction, the plasmid DNA is incubated with restriction enzymes following a standard protocol (for example NEB) to produce DNA fragments of lengths suitable for AFM imaging. Typical lengths of DNA substrates in such AFM imaging applications are between ~200 and 2000 bp. For significantly shorter DNA fragments, the measurement of structural features becomes difficult and/or inaccurate, while excessively long DNA substrates require the scanning of larger surface areas where the imaging time and/or pixel resolution become limiting. For DNA preparations starting with a PCR fragment, these DNA substrates are typically already within the desirable length range and no further restriction digest is necessary.

Homogeneous preparation of DNA fragments of uniform length can again be confirmed and the substrate at the same time purified via agarose gel electrophoresis of fluorescently stained DNA followed by gel extraction (insert in Figure 2(E)). It may be advisable to avoid exposure of the DNA to additional damaging factors such as UV irradiation, which is typically used to visualize the stained DNA bands in agarose gels. UV-induced introduction of DNA lesions at random positions within the DNA fragments can interfere with the correct interpretation of AFM data on protein–DNA interactions, especially in the context of DNA substrates for the study of protein interactions with DNA lesions. To avoid UV exposure, the gel can be separated between lane 1 and the remaining lanes, so that only lane 1 is exposed to UV light and the correct excised DNA band can then serve as a marker for the position of the specific DNA substrate in the rest of the gel when re-combining the two gel parts. The DNA is extracted from the collected gel bands following instructions of a standard kit using silica-membrane spin columns (for example NucleoSpin Extract II from Macherey-Nagel (Dueren, Germany) or Qiagen (Hilden, Germany) gel extraction kits). Importantly, the fluorescent DNA binding dye is automatically completely removed from the DNA by the DNA extraction procedure (data not shown).

Using such cheap, commercially available gel extraction kits is likely the fastest (30 min–2 h) and easiest approach for DNA purification. Alternatively, DNA substrate extraction can also be achieved from solution via phenol/chloroform or via a CsCl density gradient, as described elsewhere (Hou *et al.*, 2007; Geng *et al.*, 2011; Ristic *et al.*, 2011), with final dialysis versus a suitable storage buffer. While alcohol precipitation is likely the most simple approach for DNA purification from solution, because this method is based on aggregate formation between the negatively charged DNA and salt cations, it often results in salt contaminations on the DNA, which can pose a considerable

problem in topographical AFM experiments (Ristic *et al*., 2011). Furthermore, DNA substrate preparation based on fixing biotinylated DNA strands to streptavidin-coated magnetic beads is an elegant method that allows for easy washing and exchange of incubation solution around the immobilized DNA and for final release and elution of the purified DNA or even protein/DNA complexes using restriction enzyme digestion (Verhoeven *et al*., 2001). All these purification approaches result in considerable material losses, with typical yields varying in the broad range between 25% and 95% (own unpublished data) (Moore *et al*., 2002)[www.dnabank-network.org].

Figure 2 shows examples of AFM data on agarose gel purified DNA substrate before (A) and after modification (B). AFM imaging itself provides for the final, ultimate control of suitably clean and pure DNA substrate preparation for AFM experiments. Furthermore, quantitative analyses of the DNA samples provide information on the quality of the DNA preparation. Measurements of length distributions for DNA substrates in the images indicate the degree of sample homogeneity (Figure 2(E)). In addition, successful incorporation of target sites into the DNA can be directly investigated by AFM imaging. The binding of specific antibodies, ssDNA binding (SSB) protein, or DNA ligase to the DNA substrate can be exploited to evaluate the presence and position of specific DNA adducts, ssDNA gaps, or DNA nicks in the DNA, respectively. For instance, Figure 3(A) shows a representative AFM image of DNA fragments into which a fluorescein adduct has been introduced at 30.6% of the DNA length (as described in subsection Chemical DNA modifications), after incubation with a fluorescein antibody. Almost all of the DNA fragments show binding of the antibody at the putative position of the fluorescein (for example arrows in Figure 3(A)), confirming the presence of the fluorescein adduct in the fragments.

The DNA can be stored for months at 4 °C. Freezing the DNA is also possible, but repeated freeze-thaw cycles can result in the undesirable occurrence of dsDNA breaks. It may be advisable to avoid high salt contents in the storage buffer, which can result in the formation of micro-salt crystals on the DNA upon storage.

SAMPLE PREPARATION FOR ATOMIC FORCE MICROSCOPY IMAGING OF PROTEIN–DNA SAMPLES

For AFM imaging, protein–DNA samples have to be deposited onto a suitable substrate surface. The most commonly used substrate material for deposition of protein–DNA samples in AFM experiments is mica. We describe here briefly the properties of this substrate in the context of AFM imaging studies as well as procedures for experimental sample preparation. Extensive instructions for specific preparation of protein–DNA samples for AFM experiments have been provided previously (for example (Lyubchenko and Shlyakhtenko, 2009; Lyubchenko, 2011; Ristic *et al*., 2011)).

Atomic force microscopy substrate

The popularity of mica as an AFM substrate especially in the context of resolving minute sample particles such as protein complexes on DNA is owed to the extremely clean, flat, and smooth surface properties of this layered silicate. The typical surface roughness of mica is 0.05 nm root mean square (RMS), compared to ~0.5 nm for optimally prepared glass substrates (Fronczek *et al*., 2011). Alternatively, thoroughly cleaned silicon surfaces with roughness of $<$0.1 nm RMS have been used for deposition of DNA (Fang and Hoh, 1998). In contrast to silicon, mica requires little to no surface preparation; individual mica layers can simply be stripped off using adhesive tape to expose a surface suitable for immediate sample deposition. At physiological pH, the mica surface is negatively charged. Stable chelation of the negatively charged DNA polymers to an untreated mica surface for imaging hence requires the presence of sufficient divalent cations in solution (Pastre *et al*., 2003; Liu *et al*., 2005b; Sushko *et al*., 2006; Zhang *et al*., 2007; Pastre *et al*., 2010). In addition, different chemical modifications of the mica surface can provide positive charges for the stable attachment of the negatively charged DNA, for example, based on aminopropyltriethoxysilane or aminopropyl-silatrane chemistry (Bustamante *et al*., 1992; Shlyakhtenko *et al*., 1999; Shlyakhtenko *et al*., 2003; Liu *et al*., 2005b; Wang *et al*., 2005; Lyubchenko and Shlyakhtenko, 2009; Shlyakhtenko *et al*., 2013). These surface functionalizations can be applied either by solution or vapor deposition, as described in detail elsewhere (for example (Shlyakhtenko *et al*., 2003; Liu *et al*., 2005b; Lyubchenko and Shlyakhtenko, 2009; Shlyakhtenko *et al*., 2013)), and can provide sufficiently smooth surface roughnesses (~0.1–0.3 nm RMS (Shlyakhtenko *et al*., 2003; Lyubchenko, 2004)) to be suitable for the analysis of small structures such as DNA and protein–DNA complexes. Such substrate functionalization can be especially useful and necessary for the stable attachment of molecules for AFM imaging in liquid (see AFM Imaging Experiments on Protein-DNA Systems) (Shlyakhtenko *et al*., 2000; Hansma, 2001; Shlyakhtenko *et al*., 2003; Lyubchenko, 2004; Liu *et al*., 2005b; Lyubchenko and Shlyakhtenko, 2009; Shlyakhtenko *et al*., 2012a, 2012b; Shlyakhtenko *et al*., 2013).

Sample incubation and deposition

For experiments, protein and DNA are mixed at relevant concentrations and in a suitable incubation buffer containing the necessary co-factors for the interactions (such as for instance ATP). Often, samples can be directly incubated in a buffer solution suitable for deposition onto mica. Different proteins may, however, require different incubation concentrations, buffer conditions, or temperature, which can be adjusted to produce optimal protein activity, followed by dilution in a suitable AFM deposition buffer immediately before sample deposition. For deposition onto unfunctionalized mica, buffers for the deposition of protein–DNA samples should contain sufficient concentrations of a divalent cation (e.g. $\geq$5 mM Mg^{2+}) to chelate the negatively charged DNA polymers to the negatively charged mica surface (see section Atomic force microscopy substrate). AFM deposition buffers are ideally prepared with nanopure deionized water and filtered through a 0.02 μm pore size syringe filter (for example Anotop, Whatman) to provide a clean background for AFM imaging. For instance, Figure 3(A) shows an example of an antibody sample together with DNA containing its putative recognition site (see also in the succeeding texts, sub-section Static protein–DNA complexes). The samples were incubated at concentrations of 75 nM DNA and between 240 and 350 nM antibody at 25 °C in AFM deposition buffer (20 mM HEPES/HCl pH 8.1, 150 mM Na-acetate, 5 mM Mg-acetate) to allow binding of the antibody molecules to their target sites in the DNA (arrows in Figure 3(A)). After 30 min of incubation, the samples were diluted 50-fold in the same buffer for immediate deposition for AFM imaging to achieve

optimum surface coverage with sufficient spacing between non-interacting molecules.

Excessive amounts of free proteins on the surface lead to an increased probability of molecules being randomly located close by or even on top of DNA fragments, complicating protein–DNA interaction analyses. Different strategies have hence been employed that reduce the free protein background in the images. Wyman and colleagues have developed a powerful sample preparation technique for protein–DNA systems based on fixing of the DNA fragments to magnetic beads (Verhoeven *et al*., 2001; Verhoeven *et al*., 2002). This method allows repeated exchange of solution conditions (such as adding or removing of co-factors) and the final isolation of protein–DNA complexes for AFM deposition. Similarly, size exclusion chromatography or bead-isolation based purification of protein–DNA complexes has also been employed in EM studies (Shi *et al*., 1992; Evrin *et al*., 2009). An alternative, rapid and convenient approach for the purification of protein–DNA complexes was reported by Lyubchenko and co-workers based on spin column filtering (Shlyakhtenko *et al*., 2011; Shlyakhtenko *et al*., 2012a, 2012b). Examples of AFM images obtained on such purified protein–DNA samples are shown in Figures 3(B) and (C). Because the level of unbound protein molecules is an immediate qualitative indicator of their affinity for the DNA substrate (compare for example Figure 3(A) and Supplementary Figure S2(A)), such measures can be especially useful in the context of weakly binding protein systems. While protein systems with weaker affinity for their target sites will still dissociate from the DNA after purification (compare for example Figures 3(B) and (C)), either spontaneously or upon deposition on the mica substrate, the background of free protein molecules in these purified samples is significantly lower.

For imaging in air, the samples are rinsed with nanopure deionized water, carefully freed of excess liquid by filter paper blotting, and dried in a gentle stream of nitrogen. The rinsing step depletes the surrounding solution of free cations, leading to the stable chelation of the negatively charged polymers to the negatively charged substrate via sandwiched cations from the deposition buffer (see in the previous texts). For imaging in liquid, samples are rinsed carefully with the deposition/imaging buffer to remove loosely bound molecules, and remain covered in the buffer solution for the experiments. Compared to the water rinsing and drying of the samples for imaging in air, sample preparation for imaging in liquid does not result in as stable an attachment of the molecules onto the substrate surface. It is therefore often indispensable for imaging in liquid to apply further surface functionalization of the mica, as described previously, to enhance molecular binding to the substrate. Detailed sample preparation procedures for AFM experiments can be found elsewhere (for example (Lyubchenko and Shlyakhtenko, 2009)).

Depending on the AFM scanner system, different attachment methods for the mica plate may be required. For instance, for AFMs with a magnetic scan stage, the mica substrate is typically glued onto a magnetic disc prior to sample deposition. For imaging in air, the substrate can, for instance, easily be stably attached to a support material of choice using double-sided sticky tape or fluid glue. For imaging in liquid, the mica plate can similarly be attached to a support. However, it is important to take care that the liquid droplet on the sample surface does not get contaminated by contact with any of the surrounding material.

ATOMIC FORCE MICROSCOPY IMAGING EXPERIMENTS ON PROTEIN–DNA SYSTEMS

Atomic force microscopy experiments on protein–DNA samples offer powerful insight into the ability of a protein to recognize a particular target site. AFM imaging can be applied either in air on static samples or under near physiological, liquid environment to directly follow dynamic processes in the samples (van Noort *et al*., 1998; Hansma, 2001; Jiao *et al*., 2001; Wang *et al*., 2005). Furthermore, statistical analysis of static complexes in dried samples at different stages of an interacting system (such as protein–DNA complexes) can provide a wealth of information on dynamic processes (Janicijevic *et al*., 2003b; Crampton *et al*., 2006).

Static protein–DNA complexes

Atomic force microscopy imaging in air has been used to study many, highly diverse protein–DNA systems (Hall *et al*., 2001; Jiao *et al*., 2001; Verhoeven *et al*., 2001; Chen *et al*., 2002; Seong *et al*., 2002; Verhoeven *et al*., 2002; Janicijevic *et al*., 2003b, 2003a; Wang *et al*., 2003; Yang *et al*., 2003; Tessmer *et al*., 2005; Crampton *et al*., 2006; Wu *et al*., 2006; Tessmer *et al*., 2008; Wagner *et al*., 2009; Jiang and Marszalek, 2011; Shlyakhtenko *et al*., 2011; Roth *et al*., 2012; Shlyakhtenko *et al*., 2012a, 2012b; Tessmer *et al*., 2012). Figure 3 shows some examples of representative protein–DNA complexes. These data provide information on protein affinities to and binding positions on DNA (for example Figure 3(E)) as well as conformational properties of the complexes (for example Figures 3(F), (G) ,and (H)), from the number of protein molecules bound, their positions on the DNA, and the bend angles induced into DNA at the site of the bound protein. We will briefly describe different analytical approaches to the extraction of such quantitative information from AFM images using the examples from Figure 3. These examples are also ideally suited to point out a number of merits or caveats in AFM experiments on protein–DNA samples.

Recognition of specific target sites introduced into DNA fragments can be quantified by measuring the distances of the protein complexes on the DNA from the DNA fragment ends. For example, Figure 3(A) shows a representative AFM image of DNA fragments containing a fluorescein target site at ~31% of the fragment length of a 916 bp DNA substrate (see sub-section Chemical DNA modifications) after incubation with a fluorescein antibody (purified mouse IgG1 κ, BioLegend, see also sub-section Sample incubation and deposition). Importantly, only DNA fragments that display the correct length (within two SD from the Gaussian center of the DNA length distribution) are included in the analysis, because only for these the exact location of the target site is known. For example, the length distribution of the 916 bp DNA fragments used in these experiments is centered at ~290 nm ± 20 nm SD (Supplementary Figure S2(C)). Statistical analysis of the positions of protein complexes on the DNA fragments results in a distribution that displays a strong preference for the putative position of the fluorescein adduct as a distinct peak at ~31% of the fragment length (black bars in Figure 3(E)). In this experiment, the two DNA ends cannot be distinguished and we hence display position distributions in units of fraction of total DNA length from 0 (at the DNA fragment ends) to 0.5 (at the fragment center). Previous studies have also exploited specific structural features (ssDNA structures (Billingsley *et al*., 2012b)) at or labeling (biotinylation targeted by streptavidin marker molecules

Journal of Molecular Recognition

(Seong *et al*., 2002)) of one of the DNA ends to enable distinction between the two DNA ends and hence provide information on the polarity of the DNA template. DNA end labels can also serve experimental purposes such as an anchoring of the DNA molecules (Seong *et al*., 2002) or analytical purposes such as to provide road blocks to protein translocation (Jiang and Marszalek, 2011), and they can be introduced similar to as described previously (section Introduction of Specific DNA Sites into Long DNA Substrates).

The recognition of the target site by the antibody in this case served to confirm successful modification of the DNA (see in the previous texts, section Controls of DNA Substrate Preparations). However, typically, information on interactions with specific and non-specific DNA sites is not available for a protein system and will be the matter of investigation rather than an analytical tool. AFM is a valuable technique to obtain such binding parameters. From the position distributions of protein complexes on the DNA such as the one shown in Figure 3(E), the specificity (S) of a protein for a target site can be derived from the ratio of the areas under the Gaussian fit to the specific site population (A) and of the nonspecific background ($B = y_0 \times$ *[total fraction of DNA length]*, where y_0 is the nonspecific background height): $S = (A/B) \times N + 1$, where N is the number of available binding sites (Yang *et al*., 2005). Using the example in Figure 3(E), a Gaussian fit to the distribution gives values of $y_0 \sim 0.02$, $A \sim 0.02$, and $B \sim 0.01$, and using $N = 914$ (excluding end binding), indicates a specificity of the antibody for the fluorescein adduct of $S = 1751 \pm 215$. The data hence suggest a ~2000-fold preference of the antibody to bind to its target rather than to non-specific DNA.

As for all techniques, control experiments are essential. Staying with the example of the fluorescein antibody and the fluorescein adduct site in the DNA, experiments were repeated in the absence of antibody as well as using a DNA substrate that did not contain a fluorescein modification (Supplementary Figure S2). No binding preference was detected in either case (grey and white bars in Figure 3(E), respectively). Furthermore, the average number of protein peaks per DNA was significantly reduced for both these systems as compared to the samples of fluorescein antibody with the fluorescein modified DNA (~0.2 and 0.5 ± 0.2 protein peaks/DNA versus 1.4 ± 0.1, respectively, from three experiments each). Together, these results confirm specificity of the antibody for the fluorescein as well as successful insertion of the fluorescein adduct in the vast majority of the DNA fragments.

The position distribution in Figure 3(E) clearly shows a low number of peaks on the DNA substrate even in the absence of antibody (grey bars). These peaks are likely due to minute salt contaminations on the DNA (see also in the previous texts, subsection Controls of DNA Substrate Preparations) and will also be present as a background in the peak distributions obtained for protein–DNA samples. However, this background is both non-specific and significantly lower compared to the system of DNA containing a specific site together with a protein system with specificity to this target (fluorescein antibody and fluorescein-modified DNA; black bars in Figure 3(E)). A control protein system with no target site in the DNA indeed shows comparable density and specificity of peaks on the DNA (fluorescein antibody and non-modified DNA; white bars in Figure 3(E)), with the exception of enhanced binding to the DNA fragment ends (at fraction of DNA length from DNA end = 0). Preferences for the locally destabilized dsDNA structures at DNA fragment ends have previously been described for different DNA binding proteins (Wagner *et al*., 2009; Tessmer *et al*., 2012).

Systems with low affinity for their target sites can display many free protein molecules on the substrate surface, in addition to the DNA bound complexes. For instance, Figure 3 (A) is a representative image of a protein-DNA system with moderate affinity for its target site in the DNA in the mid to high nanomolar range. The same fluorescein antibody incubated with DNA that does not contain its target site displays a yet ~3-fold higher concentration of unbound protein molecules on the surface (Supplementary Figure S2). Figure 3(B) and (C) show AFM images obtained on protein-DNA samples with complexes that were purified prior to deposition for AFM experiments (see also sub-section Sample incubation and deposition and in the succeeding texts) and hence display less free protein molecules in the background.

From the specificity obtained from the position distribution (for example Figure 3(E)), affinities of the protein for specific (target) and non-specific sites on the DNA can be calculated, using the applied protein and DNA concentrations (Yang *et al*., 2005). Importantly, because its position on the DNA indicates whether a protein complex is bound specifically (at the target site) or non-specifically, we can distinguish these different types of complexes in the images and analyze them separately to reveal potentially different conformational or stoichiometric properties of the complexes (Chen *et al*., 2002; Wang *et al*., 2003; Tessmer *et al*., 2008).

For instance, from the volumes of particles bound to the DNA as well as unbound on the surface, protein molecular weights can be derived (Ratcliff and Erie, 2001; Wagner *et al*., 2009; Jiang and Marszalek, 2011; Roth *et al*., 2012). Such molecular weight information allows us to draw conclusions on the oligomeric state of a protein (Bao *et al*., 2003; Brar *et al*., 2008; Jiang and Marszalek, 2011; Shlyakhtenko *et al*., 2012a, 2012b) or the stoichiometry of a protein complex (Verhoeven *et al*., 2002; Roth *et al*., 2012). AFM volumes of protein peaks can be measured using different software packages (for example section tool in Igor Pro based Molecular Force Probe software, Asylum Research; ImageSXM, S. Barrett; Gwyddion, P. Klapetek and D. Nečas; Femtoscan Online, Advanced Technologies Center Moscow) and different geometrical models (Fuentes-Perez *et al*., 2013). The measured AFM volumes are typically translated into protein molecular weights via a standard linear relationship derived with a range of proteins with known molecular weights. Figure 3(F) shows an example for a volume distribution determined for the sample of ssDNA binding protein (SSB) bound to gapped DNA (Shlyakhtenko *et al*., 2012b), as shown in Figure 3(B). The single distinct peak at a volume of ~100 nm^3 in this case corresponds to a homotetrameric complex of the ~19 kDa proteins. In addition, volume calibration can also be elegantly achieved versus a second reference protein contained directly in the images (Verhoeven *et al*., 2002). This direct approach, however, requires that the protein under investigation and the control species can be easily distinguished from one another by size and/or conformation.

Finally, examples of structural analyses of protein–DNA complex conformations are shown in Figures 3(G) and (H). For instance, the DNA length distributions in Figure 3(G) indicate the degree of shortening of non-modified DNA fragments due to binding of the prokaryotic nucleotide excision repair protein complex of UvrA and UvrB (Verhoeven *et al*., 2001). The corresponding sample image is shown in Figure 3(C). DNA shortening scales linearly with the number of protein complexes bound (black bars = no protein bound, dark grey = one protein complex, and light grey = two complexes). Interestingly, the

measured DNA shortening coincides with the estimated circumference of UvrB, indicating wrapping of the DNA around the protein in the complex. A further structural feature of protein–DNA complexes that can be accessed by AFM imaging is the degree of bending of the DNA due to protein binding. Figure 3(H) shows an example for a DNA bend angle distribution determined from the sample shown in Figure 3(D) of the DNA mismatch repair protein MutS together with DNA containing a base mismatch at 27% of the DNA fragment length (Tessmer *et al*., 2008). Because the position of the mismatch in the DNA fragments is known, specific site bend angles and non-specific bend angles were determined separately. The specific site bend angles of MutS shown here clearly display a bent state with an average bend angle of about 50° as well as an unbent state (with a bend angle of 0°), which was completely absent in the non-specific complexes (Wang *et al*., 2003; Tessmer *et al*., 2008). From specific and non-specific site bend angle distributions of wild-type MutS as well as protein variants with single amino acid modifications in the two direct contacts from the protein to its target site within DNA, a model was derived for the mechanism of target site search and recognition by MutS (Tessmer *et al*., 2008). DNA bend angles and relative changes in DNA bend angles obtained from AFM experiments under different conditions and/or for different protein variants have thus provided essential information on interactions in diverse protein-DNA systems (Erie *et al*., 1994; Chen *et al*., 2002; Wang *et al*., 2003; Tessmer *et al*., 2008).

Dynamic protein–DNA interactions

Atomic force microscopy imaging in solution has been applied to resolve dynamic changes in DNA (Shlyakhtenko *et al*., 2000; Hansma, 2001; Tiner *et al*., 2001; Lyubchenko, 2004; Liu *et al*., 2005b; Jiang *et al*., 2010; Suzuki *et al*., 2010; Wang *et al*., 2010) as well as protein–DNA complexes (van Noort *et al*., 1998; Jiao *et al*., 2001; Moreno-Herrero *et al*., 2005; Zhang *et al*., 2007; Lyubchenko and Shlyakhtenko, 2009; Suzuki *et al*., 2010; Shlyakhtenko *et al*., 2012a, 2012b). Observable DNA transitions include changes in DNA condensation or supercoiling, which can be induced by protein interactions or environmental conditions (Hansma, 2001) or can reflect dynamics within the polymers (Shlyakhtenko *et al*., 2000). Dynamic studies of protein–DNA complexes most often address protein association and dissociation with as well as translocation on DNA (Hansma, 2001; Jiao *et al*., 2001; Zhang *et al*., 2007; Shlyakhtenko *et al*., 2012a, 2012b), but also DNA enzymatic degradation (Hansma, 2001), or conformational re-arrangements (Moreno-Herrero *et al*., 2005; Wang *et al*., 2005; Lyubchenko and Shlyakhtenko, 2009). The maximum time resolution of AFM scans is typically approximately 30 sec with conventional instrumental systems and conventional AFM cantilevers, depending on the imaged surface area (Hansma, 2001). Smaller cantilevers possess higher spring constants and oscillation resonance frequencies (in tapping mode), which are intrinsically linked with lower thermal noise, less damping in solution, and higher maximum scanning frequencies (Walters *et al*., 1996; Picco *et al*., 2007). Fast progress in the development of advanced, smaller cantilevers in recent years has hence enabled faster sampling rates. Furthermore, novel high speed AFM instrumentation (Ando *et al*., 2001; Ando *et al*., 2007; Picco *et al*., 2007) displays improved response times of the electronic and mechanical feedback systems and allows sub-second time resolution in the images. High speed AFM has been used to follow diverse biological processes, such as protein dynamics on DNA, protein conformational changes, protein biochemistry, and DNA folding into intricate shapes (DNA origami) (Yokokawa *et al*., 2006; Crampton *et al*., 2007; Endo *et al*., 2010; Suzuki *et al*., 2010; Shlyakhtenko *et al*., 2012a, 2012b). Figure 4 shows an example of a time series produced by high speed AFM of a DNA cytosine deaminase sliding on and dissociating from gapped DNA (Shlyakhtenko *et al*., 2012a). The DNA for these experiments was prepared using the approach described in sub-section DNA structures, using tailed DNA that was ligated together with an ssDNA fragment via bridging ssDNA adaptor segments. The enhanced time resolution of these experiments adds a further valuable dimension to the advantage of near-physiological conditions of AFM measurements in solution, making high speed AFM a highly promising emerging approach for the study of protein–DNA interactions. With time resolutions constantly improving, we can likely expect a wealth of important biological insights from dynamic AFM studies on protein-DNA interactions within the next few years.

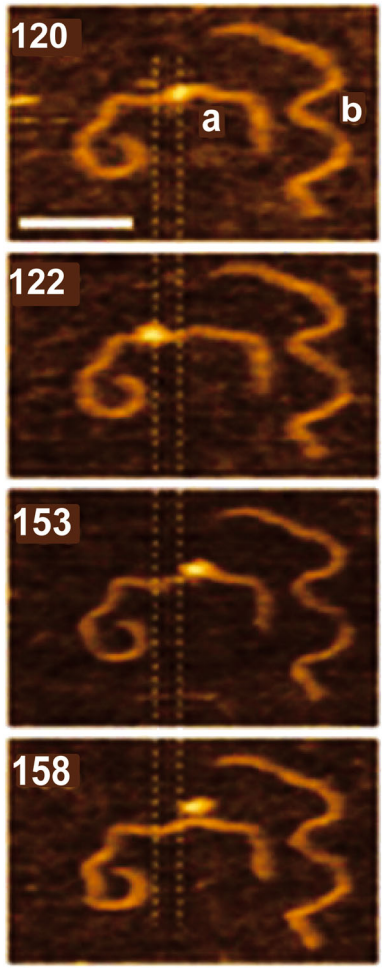

Figure 4. Atomic force microscopy time lapse series showing two DNA fragments, (a) and (b) and a single molecule of cytosine deaminase sliding on a ssDNA gap region within one of the dsDNA fragments (Shlyakhtenko *et al*., 2012a). The location of the gap in the DNA is indicated by the dashed lines. The protein dissociates upon reaching the single stranded/double stranded DNA junction. The numbers in the images indicate the frame number of the time series, collected with a time resolution of 720 ms/frame.

SUMMARY

Its high resolution at the level of the individual molecules renders AFM a powerful technique for the analysis of protein–DNA interactions. The high sensitivity of the technique and small features of protein–DNA complexes require the samples to be extremely clean. We provide here some useful advice for appropriate DNA substrate preparation for AFM imaging experiments. Moreover, we present careful preparation procedures that enable the design of DNA substrates that contain specific target sites for protein interactions. Importantly, the exact knowledge of the positions of these targets within the DNA allows us to distinguish in the images between complexes bound at the specific target site in the DNA and non-specific complexes, providing unique access to structural information on these different types of complexes.

Acknowledgments

The authors thank Samuel Wilson (National Institute of Environmental Health Sciences (NIEHS)) for initial supply of pUC19N plasmid, and Hong Wang and Florian Sauer for helpful discussions and critical reading of the manuscript. The work was supported by the Deutsche Forschungsgemeinschaft (DFG) (Rudolf Virchow Center for Experimental Biomedicine, FZ 82 to I.T).

REFERENCES

Aiyar A, Xiang Y, Leis J. 1996. Site-directed mutagenesis using overlap extension PCR. *Methods Mol. Biol.* (Clifton, N.J) **57**: 177–191.

Ando T, Kodera N, Takai E, Maruyama D, Saito K, Toda A. 2001. A high-speed atomic force microscope for studying biological macromolecules. *Proc. Natl. Acad. Sci. U. S. A.* **98**(22): 12468–12472.

Ando T, Uchihashi T, Kodera N, Yamamoto D, Taniguchi M, Miyagi A, Yamashita H. 2007. High-speed atomic force microscopy for observing dynamic biomolecular processes. *J. Mol. Recognit.* **20**(6): 448–458.

Bao KK, Wang H, Miller JK, Erie DA, Skalka AM, Wong I. 2003. Functional oligomeric state of avian sarcoma virus integrase. *J. Biol. Chem.* **278**(2): 1323–1327.

Barras F, Marinus MG. 1989. The great GATC: DNA methylation in E. coli. *Trends in Genetics: TIG* **5**(5): 139–143.

Billingsley DJ, Bonass WA, Crampton N, Kirkham J, Thomson NH. 2012a. Single-molecule studies of DNA transcription using atomic force microscopy. *Phys. Biol.* **9**(2): 021001.

Billingsley DJ, Crampton N, Kirkham J, Thomson NH, Bonass WA. 2012b. Single-stranded loops as end-label polarity markers for double-stranded linear DNA templates in atomic force microscopy. *Nucleic Acids Res.* **40**(13): e99.

Blaszak RT, Potaman V, Sinden RR, Bissler JJ. 1999. DNA structural transitions within the PKD1 gene. *Nucleic Acids Res.* **27**(13): 2610–2617.

Brar SS, Sacho EJ, Tessmer I, Croteau DL, Erie DA, Diaz M. 2008. Activation-induced deaminase, AID, is catalytically active as a monomer on single-stranded DNA. *DNA Repair* **7**(1): 77–87.

Brezeanu M, Taucher-Scholz G, Psonka K, Trager F, Hubenthal F. 2007. SFM studies of carbon ion induced damages in plasmid DNA. *J. Mol. Recognit.* **20**(6): 502–507.

Bustamante C, Rivetti C. 1996. Visualizing protein-nucleic acid interactions on a large scale with the scanning force microscope. *Annu. Rev. Biophys. Biomol. Struct.* **25**: 395–429.

Bustamante C, Vesenka J, Tang CL, Rees W, Guthold M, Keller R. 1992. Circular DNA molecules imaged in air by scanning force microscopy. *Biochemistry* **31**(1): 22–26.

Butler AP. 1986. Supercoil-dependent recognition of specific DNA sites by chromosomal protein HMG 2. *Biochem. Biophys. Res. Commun.* **138**(2): 910–916.

Chen L, Haushalter KA, Lieber CM, Verdine GL. 2002. Direct visualization of a DNA glycosylase searching for damage. *Chem. Biol.* **9**(3): 345–350.

Civit L, Fragoso A, O'Sullivan CK. 2012. Evaluation of techniques for generation of single-stranded DNA for quantitative detection. *Anal. Biochem.* **431**(2): 132–138.

Crampton N, Bonass WA, Kirkham J, Rivetti C, Thomson NH. 2006. Collision events between RNA polymerases in convergent transcription studied by atomic force microscopy. *Nucleic Acids Res.* **34**(19): 5416–5425.

Crampton N, Yokokawa M, Dryden DT, Edwardson JM, Rao DN, Takeyasu K, Yoshimura SH, Henderson RM. 2007. Fast-scan atomic force microscopy reveals that the type III restriction enzyme EcoP15I is capable of DNA translocation and looping. *Proc. Natl. Acad. Sci. U. S. A.* **104**(31): 12755–12760.

Cunningham RP, Dasgupta C, Shibata T, Radding CM. 1980. Homologous pairing in genetic-recombination - reca protein makes joint molecules of gapped circular DNA and closed circular DNA .5. *Cell* **20**(1): 223–235.

Declais AC, Lilley DM. 2008. New insight into the recognition of branched DNA structure by junction-resolving enzymes. *Curr. Opin. Struct. Biol.* **18**(1): 86–95.

Endo M, Katsuda Y, Hidaka K, Sugiyama H. 2010. Regulation of DNA methylation using different tensions of double strands constructed in a defined DNA nanostructure. *J. Am. Chem. Soc.* **132**(5): 1592–1597.

Erie DA, Yang G, Schultz HC, Bustamante C. 1994. DNA bending by Cro protein in specific and nonspecific complexes: implications for protein site recognition and specificity. *Science* (New York, N.Y.) **266**(5190): 1562–1566.

Evrin C, Clarke P, Zech J, Lurz R, Sun JC, Uhle S, Li HL, Stillman B, Speck C. 2009. A double-hexameric MCM2-7 complex is loaded onto origin DNA during licensing of eukaryotic DNA replication. *Proc. Natl. Acad. Sci. U. S. A.* **106**(48): 20240–20245.

Fang Y, Hoh JH. 1998. Surface-directed DNA condensation in the absence of soluble multivalent cations. *Nucleic Acids Res.* **26**(2): 588–593.

Fronczek DN, Quammen C, Wang H, Kisker C, Superfine R, Taylor R, Erie DA, Tessmer I. 2011. High accuracy FIONA-AFM hybrid imaging. *Ultramicroscopy* **111**(5): 350–355.

Fuentes-Perez ME, Dillingham MS, Moreno-Herrero F. 2013. AFM volumetric methods for the characterization of proteins and nucleic acids. *Methods* **60**(2): 113–121.

Geng H, Du C, Chen S, Salerno V, Manfredi C, Hsieh P. 2011. In vitro studies of DNA mismatch repair proteins. *Anal. Biochem.* **413**(2): 179–184.

Green MR, Sambrook J. 2012. Molecular Cloning: A Laboratory Manual. Cold Spring Harbor Laboratory Press, New York.

Gudowska-Nowak E, Psonka-Antonczyk K, Weron K, Elsasser T, Taucher-Scholz G. 2009. Distribution of DNA fragment sizes after irradiation with ions. *Eur. Phys. J. E Soft Matter* **30**(3): 317–324.

Hall MC, Wang H, Erie DA, Kunkel TA. 2001. High affinity cooperative DNA binding by the yeast Mlh1-Pms1 heterodimer. *J. Mol. Biol.* **312**(4): 637–647.

Hansma HG. 2001. Surface biology of DNA by atomic force microscopy. *Annu. Rev. Phys. Chem.* **52**: 71–92.

Hoeijmakers JH. 2001. Genome maintenance mechanisms for preventing cancer. *Nature* **411**(6835): 366–374.

Hou EW, Prasad R, Asagoshi K, Masaoka A, Wilson SH. 2007. Comparative assessment of plasmid and oligonucleotide DNA substrates in measurement of in vitro base excision repair activity. *Nucleic Acids Res.* **35**(17): e112.

Hu G. 1993. DNA polymerase-catalyzed addition of nontemplated extra nucleotides to the 3′ end of a DNA fragment. *DNA Cell Biol.* **12**(8): 763–770.

Janicijevic A, Sugasawa K, Shimizu Y, Hanaoka F, Wijgers N, Djurica M, Hoeijmakers JH, Wyman C. 2003a. DNA bending by the human damage recognition complex XPC-HR23B. *DNA Repair* **2**(3): 325–336.

Janicijevic A, Ristic D, Wyman C. 2003b. The molecular machines of DNA repair: scanning force microscopy analysis of their architecture. *J. Microsc.* **212**(Pt 3): 264–272.

Jeltsch A. 2002. Beyond Watson and Crick: DNA methylation and molecular enzymology of DNA methyltransferases. *Chembiochem: a Eur. J. Chem. Biol.* **3**(4): 274–293.
Jiang Y, Marszalek PE. 2011. Atomic force microscopy captures MutS tetramers initiating DNA mismatch repair. *EMBO J.* **30**(14): 2881–2893.
Jiang Y, Rabbi M, Mieczkowski PA, Marszalek PE. 2010. Separating DNA with different topologies by atomic force microscopy in comparison with gel electrophoresis. *J. Phys. Chem. B* **114**(37): 12162–12165.
Jiao Y, Cherny DI, Heim G, Jovin TM, Schaffer TE. 2001. Dynamic interactions of p53 with DNA in solution by time-lapse atomic force microscopy. *J. Mol. Biol.* **314**(2): 233–243.
Johnson AA, Akman K, Calimport SR, Wuttke D, Stolzing A, de Magalhaes JP. 2012. The role of DNA methylation in aging, rejuvenation, and age-related disease. *Rejuvenation Res.* **15**(5): 483–494.
Kelly TJ, Simancek P, Brush GS. 1998. Identification and characterization of a single-stranded DNA-binding protein from the archaeon Methanococcus jannaschii. *Proc. Natl. Acad. Sci. U. S. A.* **95**(25): 14634–14639.
Liu Y, Yang Z, Utzat CD, Liu Y, Geacintov NE, Basu AK, Zou Y. 2005a. Interactions of human replication protein A with single-stranded DNA adducts. *Biochem. J.* **385**(Pt 2): 519–526.
Liu Z, Li Z, Zhou H, Wei G, Song Y, Wang L. 2005b. Imaging DNA molecules on mica surface by atomic force microscopy in air and in liquid. *Microsc. Res. Tech.* **66**(4): 179–185.
Lushnikov AY, Brown BA, 2nd, Oussatcheva EA, Potaman VN, Sinden RR, Lyubchenko YL. 2004. Interaction of the Zalpha domain of human ADAR1 with a negatively supercoiled plasmid visualized by atomic force microscopy. *Nucleic Acids Res.* **32**(15): 4704–4712.
Luzzietti N, Brutzer H, Klaue D, Schwarz FW, Staroske W, Clausing S, Seidel R. 2011. Efficient preparation of internally modified single-molecule constructs using nicking enzymes. *Nucleic Acids Res.* **39**(3): e15.
Luzzietti N, Knappe S, Richter I, Seidel R. 2012. Nicking enzyme-based internal labeling of DNA at multiple loci. *Nat. Protoc.* **7**(4): 643–653.
Lyubchenko YL. 2004. DNA structure and dynamics: an atomic force microscopy study. *Cell Biochem. Biophys.* **41**(1): 75–98.
Lyubchenko YL. 2011. Preparation of DNA and nucleoprotein samples for AFM imaging. *Micron* **42**(2): 196–206.
Lyubchenko YL, Shlyakhtenko LS. 2009. AFM for analysis of structure and dynamics of DNA and protein-DNA complexes. *Methods* **47**(3): 206–213.
Marinus MG. 1987. DNA methylation in Escherichia coli. *Annu. Rev. Genet.* **21**: 113–131.
Mirkin SM, Frankkamenetskii MD. 1994. H-DNA and related structures. *Annu. Rev. Biophys. Biom.* **23**: 541–576.
Moore D, Dowhan D, Chory J, Ribaudo RK. 2002. Isolation and purification of large DNA restriction fragments from agarose gels. Current Protocols in Molecular Biology, 2.6.1-2.6.12.
Moreno-Herrero F, de Jager M, Dekker NH, Kanaar R, Wyman C, Dekker C. 2005. Mesoscale conformational changes in the DNA-repair complex Rad50/Mre11/Nbs1 upon binding DNA. *Nature* **437** (7057): 440–443.
Myong S, Ha T. 2010. Stepwise translocation of nucleic acid motors. *Curr. Opin. Struct. Biol.* **20**(1): 121–127.
van Noort SJ, van der Werf KO, Eker AP, Wyman C, de Grooth BG, van Hulst NF, Greve J. 1998. Direct visualization of dynamic protein-DNA interactions with a dedicated atomic force microscope. *Biophys. J.* **74**(6): 2840–2849.
Nossal NG, Makhov AM, Chastain PD, Jones CE, Griffith JD. 2007. Architecture of the bacteriophage T4 replication complex revealed with nanoscale biopointers. *J. Biol. Chem.* **282**(2): 1098–1108.
Okano M, Bell DW, Haber DA, Li E. 1999. DNA methyltransferases Dnmt3a and Dnmt3b are essential for de novo methylation and mammalian development. *Cell* **99**(3): 247–257.
Orphanides G, Reinberg D. 2002. A unified theory of gene expression. *Cell* **108**(4): 439–451.
Palmer BR, Marinus MG. 1994. The dam and dcm strains of Escherichia coli--a review. *Gene* **143**(1): 1–12.
Pastre D, Pietrement O, Fusil P, Landousy F, Jeusset J, David MO, Hamon C, Le Cam E, Zozime A. 2003. Adsorption of DNA to mica mediated by divalent counterions: a theoretical and experimental study. *Biophys. J.* **85**(4): 2507–2518.
Pastre D, Hamon L, Sorel I, Le Cam E, Curmi PA, Pietrement O. 2010. Specific DNA-protein interactions on mica investigated by atomic force microscopy. *Langmuir: ACS J. Surf. Colloids* **26**(4): 2618–2623.
Picco LM, Bozec L, Ulcinas A, Engledew DJ, Antognozzi M, Horton MA, Miles MJ. 2007. Breaking the speed limit with atomic force microscopy. *Nanotechnology* **18**(4): 044030 (4pp).
Pyle AM. 2008. Translocation and unwinding mechanisms of RNA and DNA helicases. *Annu. Rev. Biophys.* **37**: 317–336.
Ratcliff GC, Erie DA. 2001. A novel single-molecule study to determine protein--protein association constants. *J. Am. Chem. Soc.* **123**(24): 5632–5635.
Rich A, Nordheim A, Wang AHJ. 1984. The Chemistry and Biology of Left-Handed Z-DNA. *Annu. Rev. Biochem.* **53**: 791–846.
Ristic D, Modesti M, Kanaar R, Wyman C. 2003. Rad52 and Ku bind to different DNA structures produced early in double-strand break repair. *Nucleic Acids Res.* **31**(18): 5229–5237.
Ristic D, Sanchez H, Wyman C. 2011. Sample preparation for SFM imaging of DNA, proteins, and DNA-protein complexes. *Methods Mol. Biol.* (Clifton, N.J.) **783**: 213–231.
Roth HM, Romer J, Grundler V, Houten BV, Kisker C, Tessmer I. 2012. XPB helicase regulates DNA incision by the Thermoplasma acidophilum endonuclease Bax1. *DNA Repair* **11**(3): 286–293.
Sanchez H, Cardenas PP, Yoshimura SH, Takeyasu K, Alonso JC. 2008. Dynamic structures of Bacillus subtilis RecN-DNA complexes. *Nucleic Acids Res.* **36**(1): 110–120.
Seong GH, Yanagida Y, Aizawa M, Kobatake E. 2002. Atomic force microscopy identification of transcription factor NFkappaB bound to streptavidin-pin-holding DNA probe. *Anal. Biochem.* **309**(2): 241–247.
Shi Q, Thresher R, Sancar A, Griffith J. 1992. Electron-Microscopic Study of (a)Bc Excinuclease - DNA Is Sharply Bent in the Uvrb DNA Complex. *J. Mol. Biol.* **226**(2): 425–432.
Shlyakhtenko LS, Gall AA, Weimer JJ, Hawn DD, Lyubchenko YL. 1999. Atomic force microscopy imaging of DNA covalently immobilized on a functionalized mica substrate. *Biophys. J.* **77**(1): 568–576.
Shlyakhtenko LS, Potaman VN, Sinden RR, Gall AA, Lyubchenko YL. 2000. Structure and dynamics of three-way DNA junctions: atomic force microscopy studies. *Nucleic Acids Res.* **28**(18): 3472–3477.
Shlyakhtenko LS, Gall AA, Filonov A, Cerovac Z, Lushnikov A, Lyubchenko YL. 2003. Silatrane-based surface chemistry for immobilization of DNA, protein-DNA complexes and other biological materials. *Ultramicroscopy* **97**(1–4): 279–287.
Shlyakhtenko LS, Lushnikov AY, Li M, Lackey L, Harris RS, Lyubchenko YL. 2011. Atomic force microscopy studies provide direct evidence for dimerization of the HIV restriction factor APOBEC3G. *J. Biol. Chem.* **286**(5): 3387–3395.
Shlyakhtenko LS, Lushnikov AY, Miyagi A, Li M, Harris RS, Lyubchenko YL. 2012a. Nanoscale structure and dynamics of ABOBEC3G complexes with single-stranded DNA. *Biochemistry* **51**(32): 6432–6440.
Shlyakhtenko LS, Lushnikov AY, Miyagi A, Lyubchenko YL. 2012b. Specificity of binding of single-stranded DNA-binding protein to its target. *Biochemistry* **51**(7): 1500–1509.
Shlyakhtenko LS, Gall AA, Lyubchenko YL. 2013. Mica functionalization for imaging of DNA and protein-DNA complexes with atomic force microscopy. *Methods Mol. Biol.* (Clifton, N.J.) **931**: 295–312.
Slocum SL, Buss JA, Kimura Y, Bianco PR. 2007. Characterization of the ATPase activity of the Escherichia coli RecG protein reveals that the preferred cofactor is negatively supercoiled DNA. *J. Mol. Biol.* **367**(3): 647–664.
Sugasawa K, Okamoto T, Shimizu Y, Masutani C, Iwai S, Hanaoka F. 2001. A multistep damage recognition mechanism for global genomic nucleotide excision repair. *Genes Dev.* **15**(5): 507–521.
Sugasawa K, Akagi J, Nishi R, Iwai S, Hanaoka F. 2009. Two-step recognition of DNA damage for mammalian nucleotide excision repair: Directional binding of the XPC complex and DNA strand scanning. *Mol. Cell* **36**(4): 642–653.
Sushko ML, Shluger AL, Rivetti C. 2006. Simple model for DNA adsorption onto a mica surface in 1:1 and 2:1 electrolyte solutions. *Langmuir: ACS J. Surf. Colloids* **22**(18): 7678–7688.
Suzuki Y, Higuchi Y, Hizume K, Yokokawa M, Yoshimura SH, Yoshikawa K, Takeyasu K. 2010. Molecular dynamics of DNA and nucleosomes in solution studied by fast-scanning atomic force microscopy. *Ultramicroscopy* **110**(6): 682–688.
Tessmer I, Moore T, Lloyd RG, Wilson A, Erie DA, Allen S, Tendler SJ. 2005. AFM studies on the role of the protein RdgC in bacterial DNA recombination. *J. Mol. Biol.* **350**(2): 254–262.
Tessmer I, Yang Y, Zhai J, Du C, Hsieh P, Hingorani MM, Erie DA. 2008. Mechanism of MutS searching for DNA mismatches and signaling repair. *J. Biol. Chem.* **283**(52): 36646–36654.

Tessmer I, Melikishvili M, Fried MG. 2012. Cooperative cluster formation, DNA bending and base-flipping by the O6-alkylguanine-DNA alkyltransferase. *Nucleic Acids Res.* **40**(17): 8296–8308.
Tiner WJ, Sr., Potaman VN, Sinden RR, Lyubchenko YL. 2001. The structure of intramolecular triplex DNA: atomic force microscopy study. *J. Mol. Biol.* **314**(3): 353–357.
Verhoeven EE, Wyman C, Moolenaar GF, Hoeijmakers JH, Goosen N. 2001. Architecture of nucleotide excision repair complexes: DNA is wrapped by UvrB before and after damage recognition. *EMBO J.* **20**(3): 601–611.
Verhoeven EE, Wyman C, Moolenaar GF, Goosen N. 2002. The presence of two UvrB subunits in the UvrAB complex ensures damage detection in both DNA strands. *EMBO J.* **21**(15): 4196–4205.
Wagner K, Moolenaar G, van Noort J, Goosen N. 2009. Single-molecule analysis reveals two separate DNA-binding domains in the Escherichia coli UvrA dimer. *Nucleic Acids Res.* **37**(6): 1962–1972.
Walters DA, Cleveland JP, Thomson NH, Hansma PK, Wendman MA, Gurley G, Elings V. 1996. Short cantilevers for atomic force microscopy. *Rev. Sci. Instrum.* **67**(10): 3583–3590.
Wang HX, Hays JB. 2000. Preparation of DNA substrates for in vitro mismatch repair. *Mol. Biotechnol.* **15**(2): 97–104.
Wang HX, Hays JB. 2001. Simple and rapid preparation of gapped plasmid DNA for incorporation of oligomers containing specific DNA lesions. *Mol. Biotechnol.* **19**(2): 133–140.
Wang H, Yang Y, Schofield MJ, Du C, Fridman Y, Lee SD, Larson ED, Drummond JT, Alani E, Hsieh P, Erie DA. 2003. DNA bending and unbending by MutS govern mismatch recognition and specificity. *Proc. Natl. Acad. Sci. U. S. A.* **100**(25): 14822–14827.
Wang H, Bash R, Lindsay SM, Lohr D. 2005. Solution AFM studies of human Swi-Snf and its interactions with MMTV DNA and chromatin. *Biophys. J.* **89**(5): 3386–3398.
Wang X, Zhang X, Mao C, Seeman NC. 2010. Double-stranded DNA homology produces a physical signature. *Proc. Natl. Acad. Sci. U. S. A.* **107**(28): 12547–12552.
Wasserman SA, Cozzarelli NR. 1986. Biochemical topology - applications to DNA recombination and replication. *Science* (New York, N.Y) **232** (4753): 951–960.
Winzer AT, Kraft C, Bhushan S, Stepanenko V, Tessmer I. 2012. Correcting for AFM tip induced topography convolutions in protein-DNA samples. *Ultramicroscopy* **121**: 8–15.
Wu Y, Siino JS, Sugiyama T, Kowalczykowski SC. 2006. The DNA binding preference of RAD52 and RAD59 proteins: implications for RAD52 and RAD59 protein function in homologous recombination. *J. Biol. Chem.* **281**(52): 40001–40009.
Yang W. 2008. Structure and mechanism for DNA lesion recognition. *Cell Res.* **18**(1): 184–197.
Yang Y, Wang H, Erie DA. 2003. Quantitative characterization of biomolecular assemblies and interactions using atomic force microscopy. *Methods* **29**(2): 175–187.
Yang Y, Sass LE, Du C, Hsieh P, Erie DA. 2005. Determination of protein-DNA binding constants and specificities from statistical analyses of single molecules: MutS-DNA interactions. *Nucleic Acids Res.* **33**(13): 4322–4334.
Yokokawa M, Wada C, Ando T, Sakai N, Yagi A, Yoshimura SH, Takeyasu K. 2006. Fast-scanning atomic force microscopy reveals the ATP/ADP-dependent conformational changes of GroEL. *EMBO J.* **25**(19): 4567–4576.
Zhang WK, Dillingham MS, Thomas CD, Allen S, Roberts CJ, Soultanas P. 2007. Directional loading and stimulation of PcrA helicase by the replication initiator protein RepD. *J. Mol. Biol.* **371**(2): 336–348.
Zhang K, Qi H, Li H, Liu Y, Chen W. 2009. Visualization of cellular DNA crosslinks by atomic force microscopy. *Scanning* **31**(2): 75–82.
Zou Y, Walker R, Bassett H, Geacintov NE, Van Houten B. 1997. Formation of DNA repair ntermediates and incision by the ATP-dependent UvrB-UvrC endonuclease. *J. Biol. Chem.* **272**(8): 4820–4827.

SUPPORTING INFORMATION

Additional supporting information may be found in the online version of this article at the publisher's web site.

